

# Assembly History and Structure of Galactic Cold Dark Matter Halos

J. Wang<sup>1,2</sup>, J. F. Navarro<sup>3</sup>, C. S. Frenk<sup>1</sup>, S. D. M. White<sup>4</sup>, V. Springel<sup>4,5</sup>, A. Jenkins<sup>1</sup>, A. Helmi<sup>6</sup>, A. Ludlow<sup>7</sup>, and M. Vogelsberger<sup>8</sup>

<sup>1</sup> *Institute for Computational Cosmology, Dep. of Physics, Univ. of Durham, South Road, Durham DH1 3LE, UK*

<sup>2</sup> *Newton International Fellow*

<sup>3</sup> *Dep. of Physics & Astron., University of Victoria, Victoria, BC, V8P 5C2, Canada*

<sup>4</sup> *Max-Planck-Institut für Astrophysik, Karl-Schwarzschild-Straße 1, 85740 Garching bei München, Germany*

<sup>5</sup> *Heidelberg Institute for Theoretical Studies, Schloss- Wolfsbrunnenweg 35, 69118 Heidelberg, Germany*

<sup>6</sup> *Kapteyn Astronomical Institute, Univ. of Groningen, P.O. Box 800, 9700 AV Groningen, The Netherlands*

<sup>7</sup> *Argelander-Institut für Astronomie, Auf dem Hügel 71, D-53121 Bonn, Germany*

<sup>8</sup> *Harvard-Smithsonian Center for Astrophysics, 60 Garden Street, Cambridge, MA, 02138, USA*

3 September 2010

## ABSTRACT

We use the Aquarius simulation series to study the imprint of assembly history on the structure of Galaxy-mass cold dark matter halos. Our results confirm earlier work regarding the influence of mergers on the mass density profile and the inside-out growth of halos. The inner regions that contain the visible galaxies are stable since early times and are significantly affected only by major mergers. Particles accreted diffusely or in minor mergers are found predominantly in the outskirts of halos. Our analysis reveals trends that run counter to current perceptions of hierarchical halo assembly. For example, major mergers (i.e. those with progenitor mass ratios greater than 1:10) contribute little to the total mass growth of a halo, on average less than 20% for our six Aquarius halos. The bulk is contributed roughly equally by minor mergers and by “diffuse” material which is not resolved into individual objects. This is consistent with modeling based on excursion-set theory which suggests that about half of this diffuse material should not be part of a halo of *any* scale. Interestingly, the simulations themselves suggest that a significant fraction is not truly diffuse, since it was ejected from earlier halos by mergers prior to their joining the main system. The Aquarius simulations resolve halos to much lower mass scales than are expected to retain gas or form stars. These results thus confirm that most of the baryons from which visible galaxies form are accreted diffusely, rather than through mergers, and they suggest that only relatively rare major mergers will affect galaxy structure at later times.

**Key words:** cosmology: dark matter – methods: N-body simulations – Galaxy : formation

## 1 INTRODUCTION

Hierarchical growth is a signature prediction of the  $\Lambda$ CDM cosmogony, our current standard picture of cosmic structure formation.  $\Lambda$ CDM postulates a flat universe with a cosmological constant, cold dark matter, and gaussian initial conditions generated at very early times. The basic units of nonlinear structure are dark matter halos that grow by accretion and merging as gas cools and condenses into galaxies in their cores. The statistics of this process are amenable to analytic modeling, which can in turn be validated and extended through cosmological N-body

techniques (see, e.g., Press & Schechter 1974; Bond et al. 1991; Kauffmann & White 1993; Lacey & Cole 1993; Cole & Lacey 1996; Efsthathiou et al. 1988; Jenkins et al. 2001).

The mass function of collapsed structure and its evolution with time, the clustering of halos of different mass, the origin and character of scaling laws relating halo properties are all results that can be understood within the context of the excursion-set modeling making reference only to the initial power spectrum of density fluctuations and to the

universal expansion history (see, e.g., Lacey & Cole 1993; Mo & White 1996; Navarro et al. 1996).

The  $\Lambda$ CDM power spectrum,  $P(k)$ , can be computed in detail using linear theory. Under the simplifying assumption that the “temperature” of the dark matter is zero (or, equivalently, that the dark matter particle, if a thermal relic, has “infinite” mass),  $P(k)$  approaches  $k^{-3}$  on the smallest scales with a mass variance that diverges logarithmically there. Excursion-set theory then predicts that, at times of interest, effectively all of the mass of the Universe is in clumps of some mass. The assembly of a halo thus consists, in this simplified case, merely of the merging of the myriads of smaller mass subhalos that collapsed at earlier times.

Under these conditions merging is the basic engine of halo growth. The rapid mixing driven by the violently fluctuating potential of a merger has awesome transformative powers. Mergers can erase, at least partially, memory of the initial conditions and leave remnants whose broad structure is roughly independent of the cosmological conditions of formation (White 1978; van Albada 1982). Not all mergers, however, are created equal, and it has long been appreciated that the effects of major mergers differ qualitatively from those of minor events. In particular, major and minor mergers affect differently the internal structure of the remnant. Major mergers lead to “rapid growth” in the mass of an object, which has been linked with radical changes in the halo structural parameters. Minor mergers, on the other hand, are associated with “slow growth” evolutionary phases that leave the inner structure of the main halo relatively intact and affect mainly the periphery of the remnant (Salvador-Sole et al. 1998; Wechsler et al. 2002; Zhao et al. 2003; Tasitsiomi et al. 2004; Diemand et al. 2007).

The idea of merging as the exclusive mechanism of halo growth has received some backing in the literature, most recently from Madau et al. (2008), who report that most of the mass in their Via Lactea simulation of a galaxy-sized halo “is acquired in resolved discrete clumps, with no evidence for significant smooth infall”. On the other hand, a number of recent papers have also argued that the fraction of mass accreted “diffusely” might be substantial (see, e.g., Fakhouri & Ma 2010; Angulo & White 2010; Genel et al. 2010, and references therein).

Angulo & White (2010), in particular, note that when a realistic cold dark matter particle candidate is chosen its small but non-negligible thermal velocity introduces a cutoff (and finite variance) in the power spectrum on small scales that can have a profound impact on the way the evolving hierarchy of collapsed structures develops. Working through the numbers appropriate for a neutralino-dominated Universe, these authors argue that, as late as  $z \sim 20$ , most of the mass of the Universe is not yet part of *any* halo. These authors also argue that a typical galaxy-sized halo accretes at least 10% of its mass in diffuse form.

If these numbers are correct the actual fraction of smoothly-accreted material in a typical N-body halo must be much higher, since simulations can only resolve a limited range of nonlinear scales and a fair fraction of the mass is expected to be locked up in unresolved small mass clumps. Angulo & White (2010) argue that, even in the best simulations currently available, up to 30-40% of the mass of a galactic halo could have been accreted in diffuse form, in clear disagreement with the results of Madau et al. (2008). It

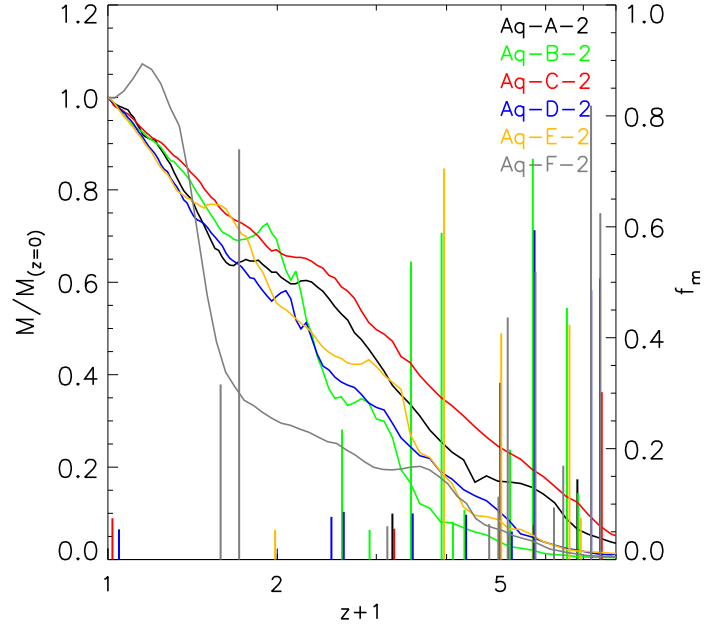


**Figure 1.** The evolution of the mass of the main friends-of-friends (FOF) progenitor of the six level-2 Aquarius halos. The curves show the mass in units of the mass at  $z = 0$  (labels on the left  $y$ -axis). Vertical segments indicate the mass ratio of the largest merger event occurring at each snapshot (labels on the right  $y$ -axis). Only merger events with mass ratio exceeding 0.05 are shown. Colors identify individual halos, as labelled in the figure. Note that only halo Aq-F-2 has undergone a major ( $f_m > 0.1$ ) merger after  $z = 1$ .

is clearly important to resolve this disagreement, especially given the importance of diffuse mass accretion for galaxy formation emphasized in recent papers (see, e.g., Kereš et al. 2005; Dekel et al. 2009, and references therein).

We address these issues here using the N-body simulations of the Aquarius Project (Springel et al. 2008). This simulation series follows the formation of six different  $\Lambda$ CDM halos at various resolutions, and includes the best-resolved galactic dark matter halo simulated so far, an object with more than one billion particles within the virial radius. We begin with a brief description of the Aquarius Project in Sec. 2, and move on in Sec. 3 to a systematic study of the radial structure of halos in terms of the mass of their progenitor halos and the time of their accretion/merging. Sec. 4 considers the mode of accretion into the halos in detail and addresses the fraction of mass accreted in diffuse form. We end with a brief summary of our main conclusions in Sec. 5.

## 2 THE NUMERICAL SIMULATIONS

The Aquarius Project (Springel et al. 2008) consists of a suite of large N-body simulations of six dark matter halos of mass consistent with that expected for the halo of the Milky Way. Our simulations assume the  $\Lambda$ CDM cosmology, with parameters consistent with the WMAP 1-year data (Spergel et al. 2003): matter density parameter,  $\Omega_M = 0.25$ ; cosmological constant term,  $\Omega_\Lambda = 0.75$ ; power spectrum nor-

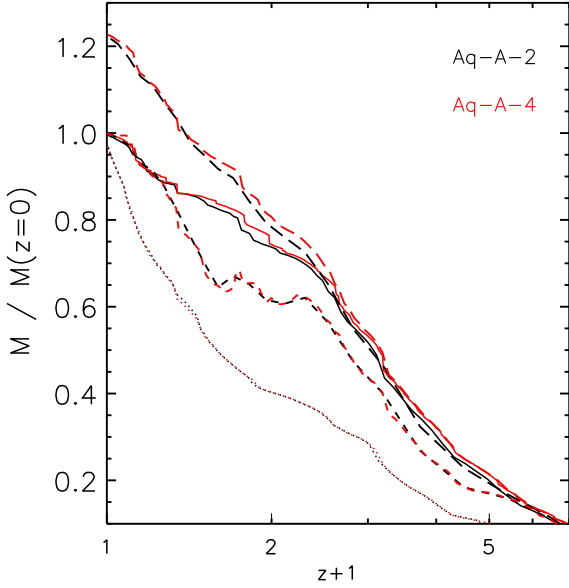


**Figure 2.** Mass accretion history of halo Aq-A. Curves in black correspond to the level-2 resolution halo, in red to the level-4 run. All masses are normalized to the FOF mass of the halo at  $z = 0$ . Four definitions of halo mass buildup are compared. The long-dashed (top) curves indicate the mass of all particles “associated” with the halo; i.e., those that were part of the main progenitor at *any time* before redshift  $z$ . The dotted (bottom) curves are the mass of particles that belong to the most massive progenitor *at all times* after  $z$  (i.e., after the time of last accretion). The thin solid curves (second set from top) indicate the cumulative mass of particles as a function of the redshift of *first* accretion into the main progenitor (regardless of whether they leave and re-enter the main progenitor subsequently). The short-dashed curves indicate the conventional FOF mass of the main progenitor at each time. This comparison illustrates the fact that a significant fraction of the mass of the main progenitor is pushed out of the halo boundary during its evolution; much of it is re-accreted later, but more than 20% is still outside the main halo at  $z = 0$ .

malisation,  $\sigma_8 = 0.9$ ; spectral slope,  $n_s = 1$ ; and Hubble parameter,  $h = 0.73$ .

The halos were identified in a  $900^3$ -particle N-body simulation of a cubic volume  $100 h^{-1}$  Mpc on a side, a lower resolution version of the Millennium-II Simulation (Boylan-Kolchin et al. 2009). This volume was resimulated using exactly the same power spectrum and phases of the original simulation, but with additional high-frequency waves added to regions surrounding the initial Lagrangian volume of each halo. The high-resolution region was populated with low-mass particles and the rest of the volume with particles of higher mass. These “zoomed-in” simulations of selected regions or individual objects have become common practice to make galaxies; for details we refer the reader to Power et al. (2003).

The six Aquarius halos are labelled “Aq-A” through “Aq-F”. Each was resimulated at different resolutions in order to assess numerical convergence. A suffix, 1 to 5, identifies the resolution level, with level 1 denoting the highest

resolution. Between levels 1 and 5, the particle mass ranges from  $m_p \sim 2 \times 10^3 M_\odot$  to  $\sim 3 \times 10^6 M_\odot$ . Level 1 was performed only for Aq-A and contains roughly 1.1 billion particles within the virial radius. All six halos were simulated at level-2 resolution. Each of these has more than 100 million particles within the virial radius.

In this study, we analyze primarily the level-2 simulations but we also use lower resolution versions of Aq-A to test for numerical convergence. For the level-2 simulations, the particle mass is  $m_p \simeq 1 \times 10^4 h^{-1} M_\odot$  and the softening length is  $\epsilon = 48 h^{-1} \text{pc}$ . At  $z = 0$ , the six haloes have a similar “virial” mass,  $M_{200} \sim 1\text{--}2 \times 10^{12} h^{-1} M_\odot$ , where  $M_{200}$  is the mass contained within  $r_{200}$ , the radius of a sphere of mean density 200 times the critical density for closure<sup>1</sup>. The circular velocity curve of the halos peaks at roughly  $V_{\text{max}} = 220 \pm 40 \text{ km s}^{-1}$ . For further details of the Aquarius Project, we refer the reader to Springel et al. (2008) and Navarro et al. (2010).

At every snapshot in the simulation we find nonlinear structures using the friends-of-friends (FOF) algorithm of Davis et al. (1985), with a linking length of 0.2 times the mean interparticle separation and 32 particles as the minimum number of particles per group. We then construct a merger tree for the final Aquarius halos linking FOF progenitors at each time. We also identify bound substructures within each FOF halo (subhalos) using the SUBFIND algorithm of Springel et al. (2005). Merger trees for subhalos are constructed as described in Springel et al. (2008).

For simplicity, unless otherwise explicitly noted, we shall identify a halo with the FOF structure that contains it. Note that the mass of FOF halos does not necessarily coincide with the virial mass alluded to above (FOF structures are larger; they typically enclose a halo and a small part of its surroundings); we shall comment on these differences when appropriate in the analysis that follows.

Fig. 1 shows the growth of the FOF mass of the main progenitor of each halo, normalized to its value at the present time,  $z = 0$ . Merger events with mass ratio greater than  $f_m = M_{\text{prog}}/M_{\text{main}} = 0.05$  are noted by vertical lines in the colour corresponding to the appropriate halo (scale on the right).

If we define the formation time of a halo as the time when the main progenitor first reaches half the final mass, then the formation time of the halos is  $z \sim 1.2\text{--}2.2$ , except for halo Aq-F-2 which is clearly different from the rest. Its formation redshift is  $z = 0.6$ , when its mass almost doubles as a result of an almost equal-mass merger (the actual mass ratio of the two progenitors is  $f_m = 0.75$ ). The other five halos have similar mass growth histories but different merger histories. For example, halos B, D, and E experienced major mergers at high redshift ( $z \sim 2\text{--}7$ ), while halos A and C grew in a relatively quiescent fashion and did not experience any major mergers after  $z = 6$ . Although the Aquarius haloes have similar final masses, they have varied formation histories, which Boylan-Kolchin et al. (2010) has shown, sample the range of behaviours seen in the Millennium II simulation for halos of this mass. The Aquarius haloes therefore provide a suitable sample to study the diver-

<sup>1</sup> This choice defines implicitly the virial radius of the halo,  $r_{200}$ , and its virial velocity,  $V_{200}$ .

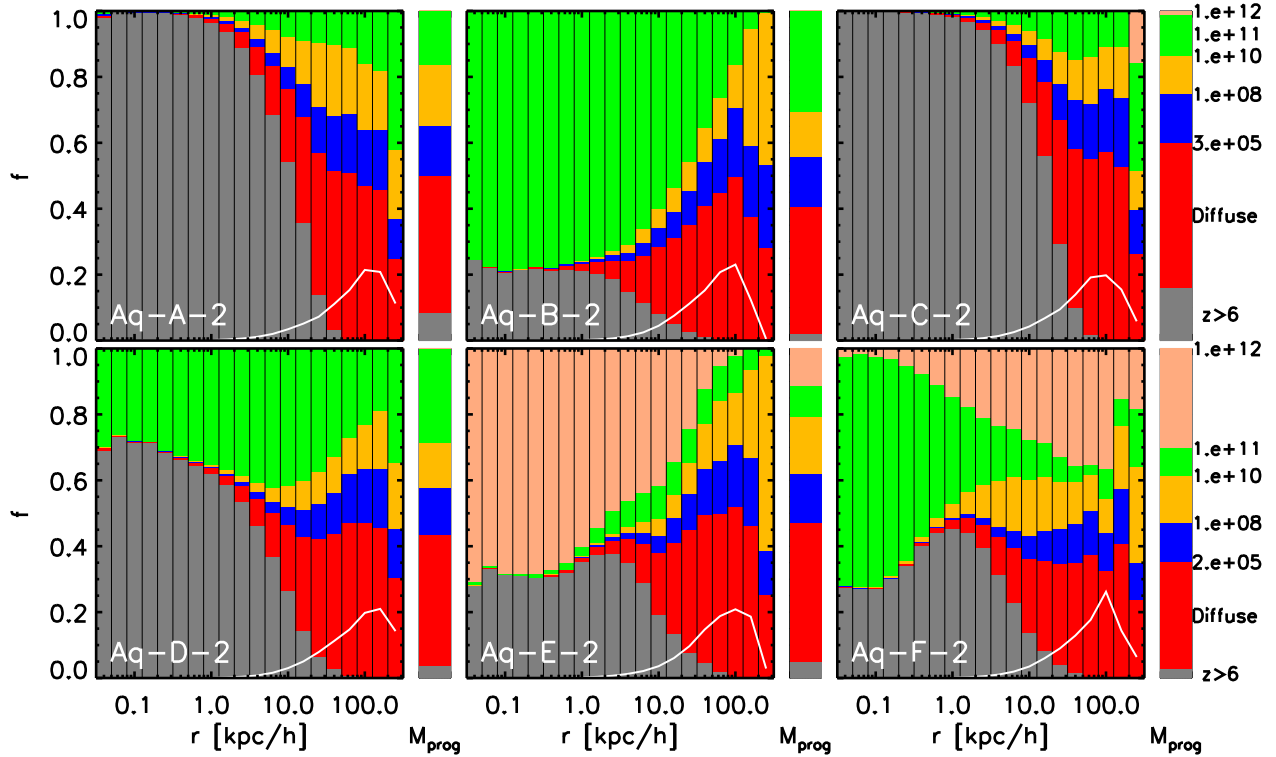


**Figure 3.** The radial distribution of particles in the FOF  $z = 0$  halo colour-coded according to  $M_{\text{prog}}$ , the mass of the progenitor to which each particle belonged at the time of (first) accretion into the main halo. The bars represent the fraction of the mass in each spherical shell brought in by halos with mass in the range indicated by the key to the right of each panel. This key also gives the total fraction (summed over all radial shells) of mass brought in by different progenitors. Material accreted before  $z = 6$  is indicated in grey. Diffuse material, that is, particles that were not part of any FOF halo at the time of accretion, are indicated in red. Masses are in units of  $h^{-1} M_{\odot}$ . The white curve gives the fraction of the total FOF halo mass in each radial shell.

sity in assembly histories of halos similar to that surrounding the Milky Way.

### 3 MASS AND ACCRETION HISTORY

#### 3.1 Mass growth and definition of accretion

Starting at  $z = 0$  we identify the main trunk of the merger tree of each of our halos by stepping back in time, defining the main progenitor at time  $n - 1$  to be the largest FOF halo which is a progenitor of the main progenitor at time  $n$ . For each particle in the final object at  $z = 0$ , we register the redshift when it was accreted into the main progenitor (i.e. when it first ceased to be a single particle or a member of *another* FOF group),  $z_{\text{acc}}$ , and the mass of the FOF group,  $M_{\text{prog}}$ , to which it belonged at the snapshot immediately preceding the time of accretion. For “diffuse” or “smooth” accretion, terms we use interchangeably throughout,  $M_{\text{prog}}$  equals the mass of a single particle.

This seemingly straightforward definition of accretion is complicated by the fact that some particles can leave the main progenitor and be re-accreted again later on. This process can actually recur multiple times, and is usually associated with accretion events, where a small but non-negligible fraction of the mass is propelled into highly energetic orbits

(Balogh et al. 2000; Gill et al. 2005; Diemand et al. 2007; Ludlow et al. 2009).

There is therefore some ambiguity in the meaning of accretion time whose effects we illustrate in Fig. 2. Here we compare the growth of halo Aq-A using several plausible definitions of accretion and two different levels of resolution to check for possible numerical artifacts. The dashed curves (second from the bottom) track, as in Fig. 1, the conventional FOF mass of the main progenitor, normalized to its value at  $z = 0$ . The long-dashed curves (top) show, on the other hand, the cumulative mass of all particles that, at any time before  $z$ , have been part of the main progenitor. These “associated” particles exceed the FOF halo at  $z = 0$  by more than 20%, highlighting the importance of the energy redistribution process described in the previous paragraph.

The solid thin curves, on the other hand, track the  $z = 0$  FOF particles, but use the time of *first* accretion to define  $z$ . The difference between this and the conventional FOF mass is a direct indicator of the accretion-escape-reaccretion process alluded to above. Finally, the dotted (bottom) curves use the time of *last* accretion of particles in the  $z = 0$  FOF group. Fig. 2 shows clearly that a halo is a dynamic object and not a static “bucket” of mass that gets progressively filled by accretion. For simplicity we shall in what follows adopt the time of first entry as our default definition of accretion but we caution that other definitions of accretion

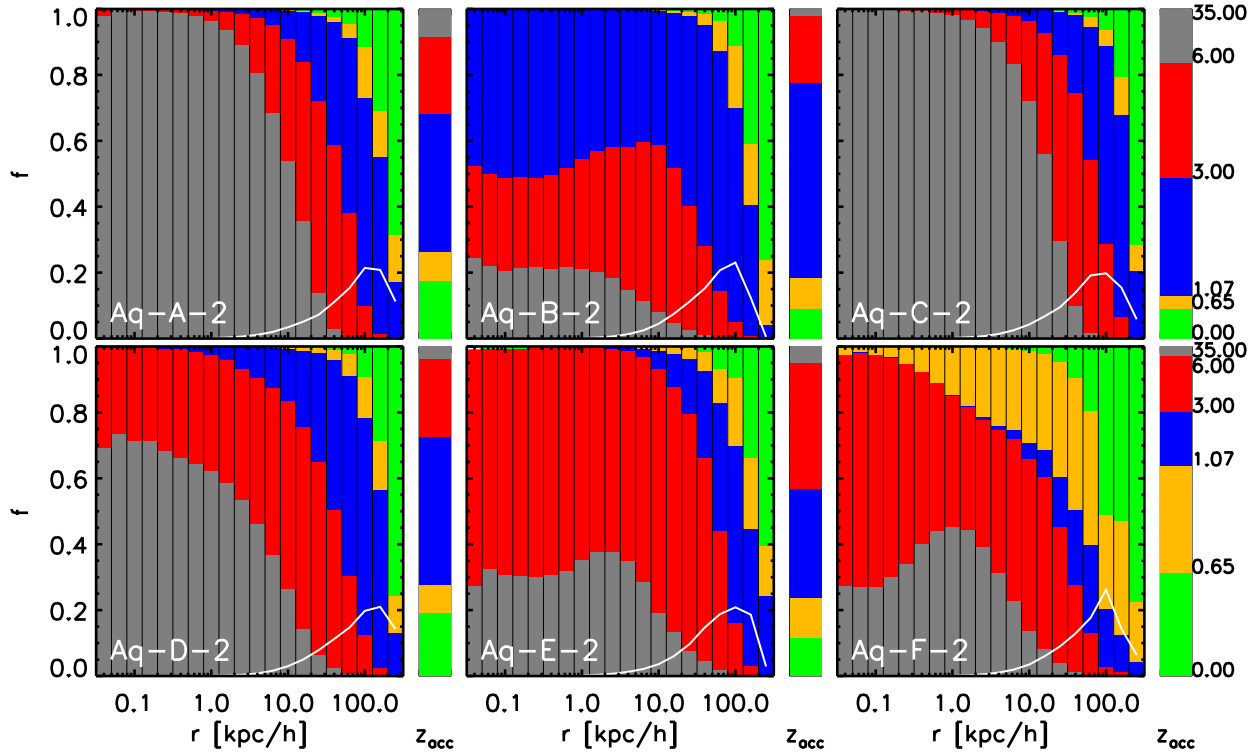


**Figure 4.** As Fig 3, but for  $z_{\text{acc}}$ , the redshift of (first) accretion of particles into the main halo. Different colours indicate accretion redshift in the intervals indicated by the key to the right of each panel. This key also gives the total mass fraction (summed over all radial shells) accreted in each redshift interval. The white curve gives the fraction of the total FOF halo mass in each radial shell.

may on occasion be more useful, depending on the aim of the analysis. The good agreement between the results for Aq-A-4 and Aq-A-2 show that these conclusions are insensitive to the numerical resolution of the simulations.

### 3.2 Progenitor mass distribution as a function of radius

We now investigate the fate of particles accreted in progenitor halos of different mass. More specifically, we investigate the distribution of halo mass in spherical shells (centred at the location of the minimum in the gravitational potential) and apportion the contribution according to the mass,  $M_{\text{prog}}$ , of the subhalos that brought each particle into the main progenitor.

This is shown in Fig. 3, which gives, in each panel, the fraction of particles in concentric radial shells of each  $z=0$  Aquarius halo, split into six mass bins, according to the mass of the progenitor halo at the time of accretion. Each bin is identified by a different colour according to the key to the right of each panel. This key, in addition, gives the total fraction (summed over all radial shells) of mass brought in by progenitors of different mass. Material that was already in place at  $z=6$  (when few resolved progenitor halos exist) is indicated in grey; in this section and the next we do not consider the assembly history at earlier times. Particles that in the snapshot preceding accretion are unattached to any resolved halo (i.e., diffuse accretion) are indicated in red.

Fig. 3 shows that there is considerable halo-to-halo variation in the mass spectrum of the progenitors of the final halo. Consider, for example, the integrated halo mass. As the key on the right of each panel shows, the fraction of mass that was already in place at  $z=6$  ranges from  $\sim 5$  to  $\sim 15\%$ . The fraction of mass accreted diffusely is substantial in all cases, ranging from  $\sim 30$  to  $\sim 40\%$ . The diffuse fraction increases with radius, from a few per cent within  $10 h^{-1} \text{ kpc}$ , to more than 20 per cent within  $100 h^{-1} \text{ kpc}$ . This agrees with the results found by Helmi et al. (2002) from an N-body simulation of a cluster halo scaled to a galactic mass. The radial behaviour is diverse. For example, in halos A and C the material in the innermost region,  $r < 1 \text{ kpc}$ , was already in place before  $z=6$  and has undergone little change since. By contrast, in halos B, E and F, most of the central mass was brought in after  $z=6$  through mergers involving host halos with mass greater than  $10^{10} h^{-1} M_{\odot}$ .

Halo D is intermediate between these two extremes. Large progenitors, of mass  $> 10^{10} h^{-1} M_{\odot}$ , bring in between 20 and 40% of the final mass at all radii. In general, the larger the mass of the carrier halo, the greater the probability of the particles ending up in the central regions. Very little of the diffuse material makes it into the central regions,  $r < 10 h^{-1} \text{ kpc}$ ; indeed, most of it stays in the outer regions where it typically contributes most of the mass.



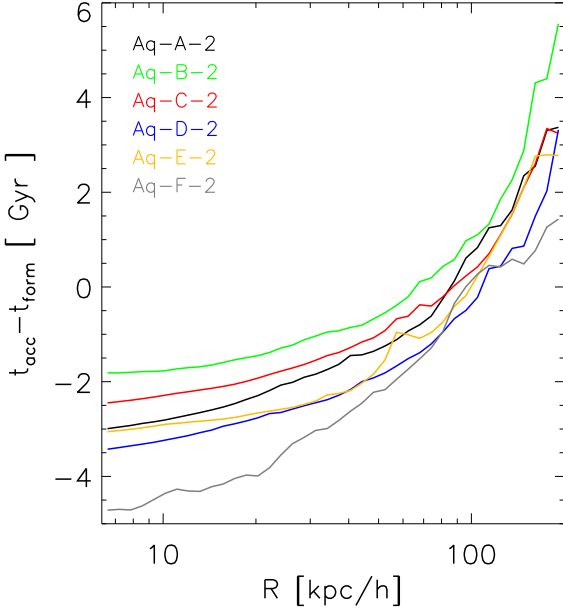


**Figure 5.** The mean accretion time of particles in different radial shells at  $z = 0$ . Accretion times are shown relative to the formation time of each halo,  $t_{\text{form}}$ , defined as the time when the halo first reached half its final mass. When defined this way the mean accretion time profile is similar for all Aquarius halos.

### 3.3 Accretion time distribution as a function of radius

We now turn our attention to the radial distribution of particles as a function of their accretion time. Analogously to Fig. 3, Fig. 4 shows the distribution of accretion redshifts, binned according to distance to the centre of the halo. In each radial shell, the contribution from material accreted in different time intervals is shown by strips coloured according to the key shown to the right of each panel. The key also gives the fractions of the total halo mass (summed over all shells) accreted in each redshift interval.

The inside-out nature of halo assembly is clearly apparent in Fig. 4. On average, the peak contribution from each accretion redshift interval marches outwards with time. The inner regions are populated mostly by particles that were accreted early; the outer layers were added gradually later. The cores of halo A and C were in place before  $z = 6$  and evolved little thereafter. In halos D, E, and F, the core particles were accreted by  $z = 3$ , but for halo B, the core is accreted at  $z = 1$  because two major mergers in the redshift interval  $1 < z < 3$  bring in almost 50% of the core mass (see Fig. 1). These mergers happen relatively early, while the total halo mass is small, and disrupt the original core which then reforms from the new material. By contrast, the late major merger undergone by halo F has a relatively minor effect on the core, probably because of the orbital parameters of the merger. The core in this case is actually made primarily out of material that was accreted in earlier, lesser mergers at  $z \sim 4$ .

The radial dependence of accretion time is quantified

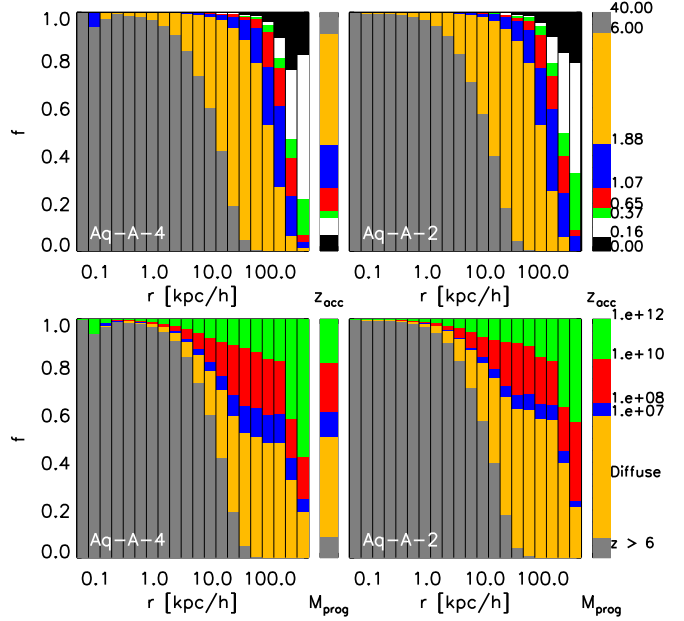


**Figure 6.** A convergence test of the radial gradients in progenitor mass and accretion redshift. The top two panels are analogous to Fig. 4, the bottom panels to Fig. 3, but for the level-2 and level-4 Aq-A runs. These runs differ solely in numerical resolution; level-2 runs have  $30\times$  more particles and  $5\times$  smaller gravitational softening than their level-4 counterparts. The excellent agreement shows that the results presented in Figs. 3 and 4 are insensitive to numerical resolution.

further in Fig. 5, which shows the average accretion time as a function of radius. Accretion time is plotted relative to the formation time of the halo,  $t_{\text{form}}$ , defined as the time when the main progenitor first reaches half its final mass. With this normalization, the radial dependence of the accretion time is fairly similar for all Aquarius halos. On average, the material in the inner  $10 h^{-1} \text{ kpc}$  is assembled 2 to 4 Gyr before  $t_{\text{form}}$  whereas the material beyond  $100 h^{-1} \text{ kpc}$  falls in 2 to 4 Gyr after  $t_{\text{form}}$ . This onion-like growth is generic for cold dark matter halos of galactic scale; it was seen also in a scaled cluster N-body simulation by Helmi et al. (2003).

### 3.4 Numerical convergence

Before discussing these results further we should verify that the trends presented above are not unduly influenced by numerical resolution. The availability of simulations of the same halo at varying resolution allows for direct testing of the reliability of our results. We do this by comparing the level-2 simulation of halo Aq-A, which is the one we have analyzed so far, with its level-4 counterpart. The level-4 simulation has about  $30\times$  poorer mass resolution and  $5\times$  poorer spatial resolution (softening).

The test is carried out in Fig. 6, which shows the distributions of accretion time and the mass spectrum of progenitor halos as a function of radius. These figures are analogous to Figs. 3 and 4. Panels on the left show the level-4 results, those on the right the level-2 results. It is clear that the

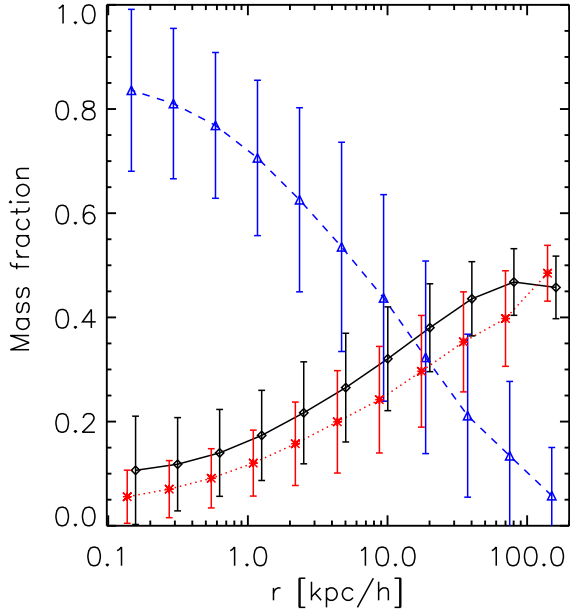


**Figure 7.** The fraction of particles in a series of spherical shells that were accreted smoothly (black circles – solid line), by minor mergers (starred symbols – dotted) and by major mergers (open triangles – dashed). The distinction between minor and major mergers is made at a mass ratio of 10:1. Fractions are averaged over all six level-2 Aquarius halos and error bars show the *rms* scatter among halos. Despite substantial scatter, the trends are clear. Major mergers contribute to the inner regions, diffuse accretion and minor mergers mainly to the outer regions which contain the bulk of the mass.

convergence of these properties is excellent. There is no discernible difference in the distributions of  $z_{\text{acc}}$  and at most a  $\sim 10\%$  difference in the distributions of  $M_{\text{prog}}$  in the lowest mass range,  $M_{\text{prog}} < 10^7 h^{-1} M_{\odot}$ .

## 4 MODES OF ACCRETION

In this section we study how the growth of halos is apportioned between major mergers, minor mergers, and smooth accretion; how the material added in these modes is distributed in radius in the final halos; and how much variation there is between halos. We will adopt a FOF mass ratio of 10:1 as our standard division between major and minor mergers, although we will also give some results for the stricter 3:1 ratio adopted as a boundary by some authors. The fact that we limit our FOF group catalogues to systems with at least 32 particles means that the boundary between minor mergers and “smooth” accretion occurs at a mass ratio of about  $10^{6.5}:1$  at  $z = 0$  dropping to about  $10^{5.5}:1$  at  $z = 4$  and to even smaller values at higher redshifts. In this section we consider increases in mass through each of these growth modes throughout the entire history of each halo, rather than halting at  $z = 6$  as in previous sections.

### 4.1 Major mergers vs minor mergers

In Fig. 7 we illustrate how major mergers, minor mergers and diffuse accretion contribute to the  $z = 0$  mass in a series of spherical shells, each spanning a factor of two in radius. The symbols joined by lines give results averaged across the six Aquarius halos, while the error bars indicate the *rms* scatter among halos. Within  $\sim 10 h^{-1}$  kpc, major mergers are the dominant source of the material, providing typically 40% of the mass, while minor mergers and smooth accretion bring in about 30% each respectively; within  $\sim 1.0 h^{-1}$  kpc, major mergers contribute more than two thirds of the mass. Note, however, that less than 10% of halo mass lies within  $\sim 10 h^{-1}$  kpc and less than 1% lies within  $\sim 1.0 h^{-1}$  kpc. Note also from Fig. 4 that the great majority of these major mergers occurred at  $z > 3$  and many of them at  $z > 6$ . Only in halos B and F are there substantial contributions to these regions from major mergers at redshifts below 3. The large error bars on these points indicate that the scatter of the major merger contribution to the inner regions of halos is large.

Beyond  $10 h^{-1}$  kpc, in the region which contains the bulk of the halo mass, both minor mergers and diffuse accretion contribute more to halo growth than major mergers. Indeed, averaged over all six halos, major mergers contribute only 17% of the total mass growth, with the values for individual halos ranging from 3% (Aq-A) to 36% (Aq-F). For a stricter definition of a major merger, requiring a mass ratio of 3:1 or less, the mean major merger contribution drops to just 9%, with individual values ranging from  $< 0.1\%$  (Aq-A, Aq-C) to 25% (Aq-F). Thus, major mergers are typically a small contribution to overall halo growth. The rest is split almost evenly between minor mergers and “diffuse” accretion. It is interesting that the scatter in each of these contributions is very close to half that in the major merger contribution. This shows that the minor merger and diffuse fractions fluctuate up and down together, with minor mergers contributing slightly less than half of the material not accounted for by major mergers at each radius and in each halo.

### 4.2 Diffuse accretion

Given the conflicting claims in the literature regarding the importance of diffuse accretion discussed in the Introduction, it is important to explore possible biases and subtleties involved in reckoning the amount of diffuse mass accreted. The dynamic nature of halo buildup highlighted above (Sec. 3.1) introduces ambiguities in the meaning of accretion, so we compare four alternative definitions of  $f_{\text{smooth}}$ , the total fraction of mass in the FOF halo at  $z = 0$  that has been added smoothly:

- I: all particles that were not part of *any* 32+ particle FOF group *in the snapshot immediately before* the time of first accretion,  $z_{\text{acc}}$ ;
- II: all particles that were never part of *any* 32+ particle *bound* structure (as identified by SUBFIND) before  $z_{\text{acc}}$ ;
- III. same as (II) but for 20+ particles;
- IV: same as (I) but for *all* snapshots before  $z_{\text{acc}}$ .

Fig. 8 compares results for the six level-2 Aquarius halos. Criterion (I), probably the simplest, is seen to give the largest estimate of  $f_{\text{smooth}}$  in all cases. This criterion omits

those particles that were part of FOF halos in the past, but that have left them and are unattached to any resolved structure just before accretion. These make a surprisingly large fraction (about *half*!) of the smooth fraction computed using criterion (I), as shown by the bottom curve corresponding to criterion (IV).

One shortcoming of criterion (IV), however, is the possibility that FOF groups may artificially link in physically unrelated particles. This is especially true in small- $N$  groups (for a recent discussion, see, e.g., Bett et al. 2007). Criteria (II) and (III) account for this by requiring particles to be part of *bound* structures; varying the threshold from 20 to 32 particles has negligible effect on the results. This extra condition is seen to increase  $f_{\text{smooth}}$  by roughly 50% relative to criterion (IV). The contribution of diffuse accretion seems, therefore, to be genuinely high, between 20 and 40% of the final halo mass overall.

We note that, strictly speaking,  $f_{\text{smooth}}$  depends on the total number of snapshots used in its estimation. The numbers quoted above are based on a total of 128 snapshots, but for one of the runs (Aq-A-2) data were stored for 1024 snapshots. The estimate of  $f_{\text{smooth}}$  according to criterion (I) changes little when considering 1024 or 128 snapshots: from 41% to just 36%. The changes are even smaller for definitions II or III.

Finally, we consider the dependence of  $f_{\text{smooth}}$  on the mass resolution of the simulations. For this, we use four different realizations of halo Aq-A, from level 2 to level 5. The results are shown in Fig. 9 (criteria II and IV: open diamonds and asterisks, respectively). As expected, there is a systematic decrease in  $f_{\text{smooth}}$  with increasing resolution, measured in Fig. 9 by  $M_{\text{cut}}$ , the mass of a group of 20 particles.

Given that  $f_{\text{smooth}}$  depends on resolution, we need to ask how secure is our estimate of this quantity from the simulations. We can answer this by analyzing Monte Carlo merger trees built using the excursion-set formalism, constrained at  $z = 0$  to make a halo of mass comparable to those in the Aquarius set. In particular, we use the algorithms of Parkinson et al. (2008) and Cole et al. (2008), which were tuned to match the N-body merger trees of the Millennium Simulation (Springel et al. 2005). This approach has the advantage that a cutoff mass can be easily introduced in order to mimic the limited resolution of a simulation (see, e.g., Angulo & White 2010).

The excursion-set results are shown by the dotted line in Fig. 8 and by the connected dots in Fig. 9. The Monte Carlo trees, when trimmed to match the resolution of the N-body simulations, give results in good agreement with the simulations. The theoretical calculation also confirms the large scatter in  $f_{\text{smooth}}$  seen in the simulations. (The “error bars” on the Monte Carlo results denote the *rms* scatter among several hundred realizations.)

The trends shown in Fig. 9 imply that further improvements in resolution would result in only small reductions in the value of  $f_{\text{smooth}}$ . Indeed,  $f_{\text{smooth}}$  seems to depend more strongly on the particular definition adopted for smooth accretion than on numerical resolution, at least for the 100-million particle halos we consider here. The vertical line in Fig. 9 shows the value of  $M_{\text{cut}}$  corresponding to Aq-A-1, the best-resolved, billion-particle halo in the Aquarius set. The Monte Carlo tree results suggest that its additional res-

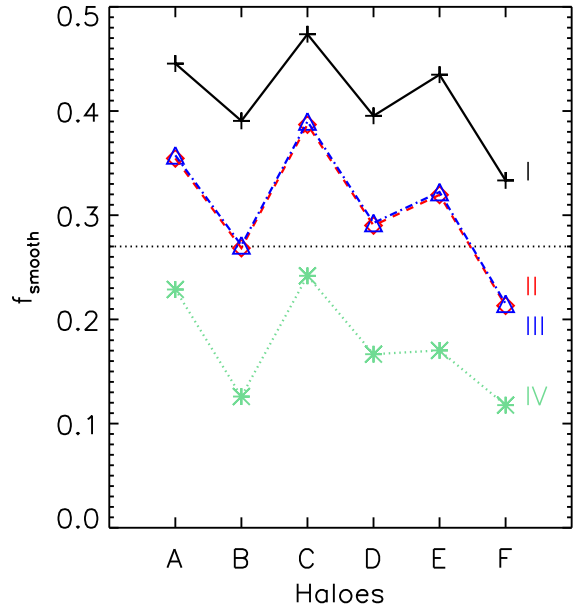


**Figure 8.** The fraction of mass accreted in diffuse form in each level-2 Aquarius halo. The  $x$ -axis lists the name of each halo. Each curve corresponds to one of the definitions of “diffuse accretion” introduced in the text. Briefly, (I) are particles that are unattached to any FOF group identified in the snapshot immediately before first accretion; (II) refers to particles that do not belong to any *bound* structure with  $\geq 32$  members in *any* snapshot before first accretion; (III) is as (II) but for 20 members; and (IV) denotes material that did not belong to *any*  $N \geq 32$  FOF group at any time before first accretion. All curves use a total of 128 snapshots to estimate  $f_{\text{smooth}}$ . The excursion-set prediction for a halo of the same mass and comparable numerical resolution is shown by the horizontal dotted line.

olution would result in only a very small decrease in the smoothly accreted fraction.<sup>2</sup>

We conclude from this exercise that the substantial fraction of mass found to be accreted smoothly in our simulations is a robust result. We can therefore confidently rule out the claim by Madau et al. (2008) that at most 3% of the mass of a galaxy-sized halo can be supplied by smooth accretion. It is not clear at this point what the cause of the disagreement is, but it is likely to be related to the way in which these authors compute diffuse accretion rather than to differences in the simulations themselves. For example, the mass they regard as having been accreted in “identifiable subunits” is just the sum of the masses of all progenitor halos that contain particles that make it into the final system. A substantial fraction of that summed mass includes particles that are *not* part of the halo at  $z = 0$ ; this could have led Madau et al. (2008) to overestimate the mass contributed by discrete identifiable subunits and, therefore, to underestimate  $f_{\text{smooth}}$ .

<sup>2</sup> We have not attempted the analysis presented here for Aq-A-1 because of the formidable computational task involved in building full merger trees for this simulation.



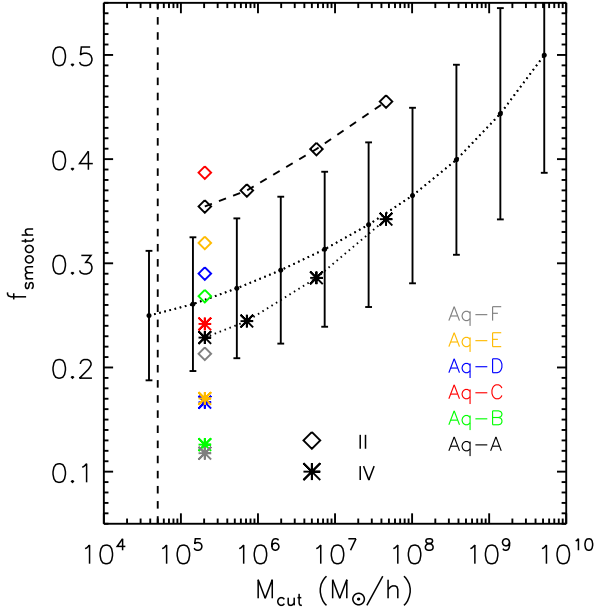


**Figure 9.** The dependence of the diffuse accretion fraction,  $f_{\text{smooth}}$ , on the mass resolution of the simulations,  $M_{\text{cut}}$ , defined as the mass of a group of 20 particles. Open diamonds and asterisks refer to diffuse accretion definitions II and IV, as described in the text and in the caption to Fig. 8. Connected symbols refer to resolution levels 2 through 5 for halo Aq-A. Colors indicate different halos, as labelled in the panel. Dots with error bars indicate the mean and  $rms$  scatter in several hundred Monte Carlo assembly histories constructed from excursion-set theory. The vertical dotted line indicates the value of  $M_{\text{cut}}$  for Aq-A-1, the highest resolution simulation in the Aquarius series.

Our conclusions are in agreement with those of Angulo & White (2010) (see also Genel et al. 2010): mergers and smooth accretion are both defining features of the hierarchical buildup of a CDM halo.

At redshifts  $z \leq 6$  the intergalactic medium is fully photoionized and gas is unable to collect in halos with maximum circular velocity below about 15 km/s, corresponding to masses below roughly  $10^8 M_{\odot}$  (Okamoto et al. 2008). This is well above the resolution limit of our simulations, so the gas associated with these low-mass halos should be considered to be diffusely accreted along with that associated with the “diffuse” dark matter. Taking the limit at exactly  $10^8 h^{-1} M_{\odot}$  for simplicity<sup>3</sup>, we find that, on average, our halos accrete 56% of their baryons diffusely, with the numbers for individual halos ranging from 46% (Aq-F) to 64% (Aq-C). The bulk of baryonic accretion is thus predicted to be smooth rather than clumpy for objects of Milky Way scale.

### 4.3 Evolution of the inner mass profile

As Fig. 7 indicates, major mergers contribute, on average, just under half of the particles in the inner  $10 h^{-1}$  kpc of Galactic halos. This is the region occupied by the luminous

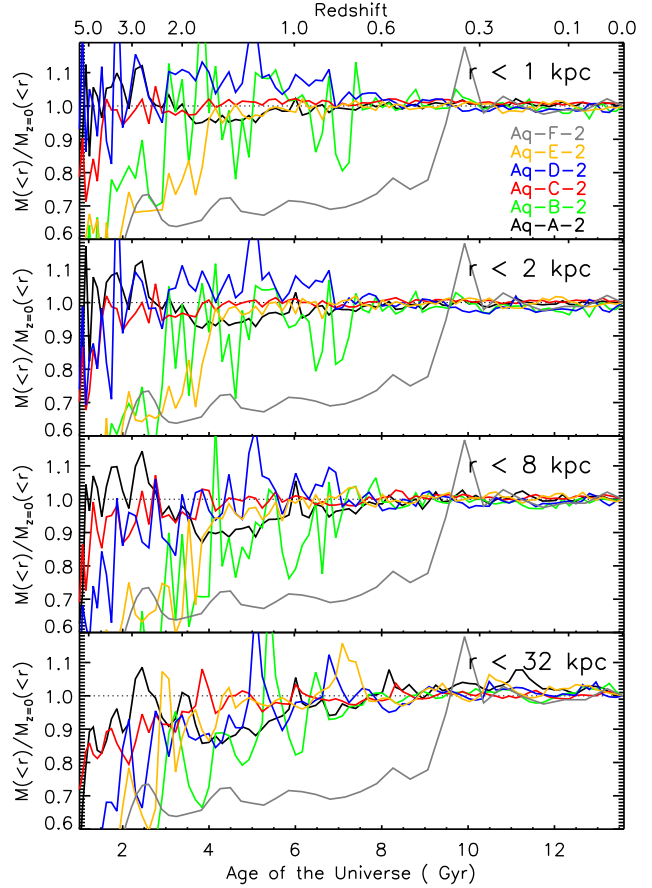


**Figure 10.** Total mass enclosed within different physical radii,  $M(<r)$ , for  $r = 1; 2; 8$ ; and  $32$  kpc, as a function of cosmic time. Different colours correspond to different halos, as labelled in the figure. Masses in each panel are normalized to their values at  $z = 0$ . Time is labelled at the bottom, redshift at the top. Except for halo Aq-F, which is the remnant of a recent major merger, the inner mass profile of Aquarius halos has been very stable for the past 5–6 Gyr, a period comparable to the age of the Solar System.

component of the central galaxy, and it is thus interesting to analyze in detail how the mass profile in this region evolves with time. A thin stellar disk, for example, could react to clumpy addition of material by thickening and becoming dynamically hotter, potentially violating observations of the thin disk in the solar neighbourhood (see e.g. Benson et al. 2004).

We investigate the stability of the inner halo explicitly in Fig. 10, where we plot the mass enclosed within 1, 2, 8, and 32 (physical) kpc<sup>4</sup> from the centre of each halo as a function of time. Each curve is normalized to the enclosed mass at  $z = 0$ . Except for halo F, which undergoes a major merger at  $z \sim 0.6$ , all the halos show exceptionally stable inner mass profiles over at least the past 5 Gyr ( $z < 0.6$ ), the age of the Solar System. Five out of six Aquarius halos could, in principle, host a disk as thin and cold as that of the Milky Way. Late-accreted mass typically settles in the

<sup>3</sup> The following numbers are insensitive to this choice.

<sup>4</sup> We assume  $h = 0.73$  in order to compare with observations of the Milky Way.

outskirts of a halo, thus allowing the hierarchical growth of halos to be reconciled with the ubiquitous presence of thin stellar disks.

## 5 SUMMARY AND CONCLUSIONS

We have analyzed the build-up of six  $\Lambda$ CDM halos simulated as part of the Aquarius Project to study the influence of assembly history on halo structure. We focus on the distributions of progenitor mass and accretion time for particles at different radii at the final time, and discuss various plausible definitions of accretion time, together with the difficulties involved in estimating the total mass fraction accreted smoothly. We compare simulations of the same halo carried out with different resolution in order to assess the sensitivity of our results to numerical limitations.

Although there is considerable variation from halo to halo, our simulations exhibit a number of very clear trends. Our main conclusions may be summarized as follows.

- There is a strong radial gradient in accretion time, which confirms that halos are built from the inside out. Later accreting material settles farther from the centre of the halo; particles that today reside inside  $10 h^{-1}$  kpc are typically accreted  $\sim 3$  Gyr earlier than particles that reside at  $100 h^{-1}$  kpc from the centre.
- Similarly strong correlations exist between distance of a particle from halo centre and the mass at accretion of the progenitor halo which contained it. The innermost regions are dominated by particles brought in by massive clumps, “major mergers” with mass ratios exceeding 1:10, as well as by those that joined the main progenitor at very early times ( $z > 6$ ). Mass accreted diffusely and in minor mergers predominantly populates the more distant parts of the halo and dominates the total mass.
- Minor mergers and diffuse accretion contribute approximately equally to the mass of each halo at each radius, at least at the resolution of our six Aquarius halos where minor mergers can be distinguished up to mass ratios exceeding  $10^6:1$ .
- The inner mass profile of a halo is very stable at late times in systems that stay clear of major mergers. In five of the six Aquarius halos the profile within 32 kpc barely changes in the past 5-6 Gyr.
- Diffuse accretion contributes a substantive fraction of the final mass of the halo, roughly 30-40% in our simulations. This is a robust result compatible with expectations from excursion-set modeling.
- Our analysis shows that some of the material accreted smoothly had previously been part of other collapsed structures, from which it was probably ejected by mergers. The same mechanism leads a fair fraction of particles in the main halo to cycle in and out of its main progenitor; at  $z = 0$  the cumulative mass of all particles “associated” in the past with the main progenitor exceeds the final mass of the halo by at least 20%.
- After reionization, gas is unable to collect in dark halos with masses lower than about  $10^8 h^{-1} M_\odot$ . As a result more than half of all the baryons associated with halos of Milky Way scale are expected to be accreted smoothly, rather than in clumps.

These results emphasize the dynamic nature of halo buildup and provide insight into the radial structure of a halo and the history of its assembly process. The view that emerges highlights some misconceptions regarding hierarchical growth. CDM halos are not passive repositories where mass is added in continuous but discrete events, but rather lively systems that can lose as well as gain material throughout their lifetimes. Diffuse accretion, recurring infall, escape and fallback, are all processes that play important roles in the build-up of CDM halos.

## ACKNOWLEDGEMENTS

The simulations of the Aquarius Project were carried out at the Leibniz Computing Center, Garching, Germany, at the Computing Centre of the Max-Planck-Society in Garching, at the Institute for Computational Cosmology in Durham, and on the ‘STELLA’ supercomputer of the LOFAR experiment at the University of Groningen. We thank Shaun Cole for providing us the code to produce Monte Carlo merger trees, and Mike Boylan-Kolchin for useful comments and careful reading of the manuscript. JW acknowledges a Royal Society Newton International Fellowship, CSF a Royal Society Wolfson Research Merit Award and AH support from a VIDI grant by Netherlands Organisation for Scientific Research (NWO). AH acknowledges funding from the European Research Council under ERC-StG GALACTICA-240271. This work was supported by an STFC rolling grant to the Institute for Computational Cosmology.

This paper has been typeset from a  $\text{\LaTeX}$  file prepared by the author.

## REFERENCES

- Angulo R. E., White S. D. M., 2010, *MNRAS*, 401, 1796  
 Balogh M. L., Navarro J. F., Morris S. L., 2000, *ApJ*, 540, 113  
 Benson A. J., Lacey C. G., Frenk C. S., Baugh C. M., Cole S., 2004, *MNRAS*, 351, 1215  
 Bett P., Eke V., Frenk C. S., Jenkins A., Helly J., Navarro J., 2007, *MNRAS*, 376, 215  
 Bond J. R., Cole S., Efstathiou G., Kaiser N., 1991, *ApJ*, 379, 440  
 Boylan-Kolchin M., Springel V., White S. D. M., Jenkins A., 2010, *MNRAS*, 406, 896  
 Boylan-Kolchin M., Springel V., White S. D. M., Jenkins A., Lemson G., 2009, *MNRAS*, 398, 1150  
 Cole S., Helly J., Frenk C. S., Parkinson H., 2008, *MNRAS*, 383, 546  
 Cole S., Lacey C., 1996, *MNRAS*, 281, 716  
 Davis M., Efstathiou G., Frenk C. S., White S. D. M., 1985, *ApJ*, 292, 371  
 Dekel A., Birnboim Y., Engel G., Freundlich J., Goerdt T., Mumcuoglu M., Neistein E., Pichon C., Teyssier R., Zinger E., 2009, *Nature*, 457, 451  
 Diemand J., Kuhlen M., Madau P., 2007, *ApJ*, 667, 859  
 Efstathiou G., Frenk C. S., White S. D. M., Davis M., 1988, *MNRAS*, 235, 715  
 Fakhouri O., Ma C., 2010, *MNRAS*, 401, 2245

- Genel S., Bouché N., Naab T., Sternberg A., Genzel R., 2010, *ApJ*, 719, 229
- Gill S. P. D., Knebe A., Gibson B. K., 2005, *MNRAS*, 356, 1327
- Helmi A., White S. D., Springel V., 2002, *Phys. Rev. D*, 66, 063502
- Helmi A., White S. D. M., Springel V., 2003, *MNRAS*, 339, 834
- Jenkins A., Frenk C. S., White S. D. M., Colberg J. M., Cole S., Evrard A. E., Couchman H. M. P., Yoshida N., 2001, *MNRAS*, 321, 372
- Kauffmann G., White S. D. M., 1993, *MNRAS*, 261, 921
- Kereš D., Katz N., Weinberg D. H., Davé R., 2005, *MNRAS*, 363, 2
- Lacey C., Cole S., 1993, *MNRAS*, 262, 627
- Ludlow A. D., Navarro J. F., Springel V., Jenkins A., Frenk C. S., Helmi A., 2009, *ApJ*, 692, 931
- Madau P., Diemand J., Kuhlen M., 2008, *ApJ*, 679, 1260
- Mo H. J., White S. D. M., 1996, *MNRAS*, 282, 347
- Navarro J. F., Frenk C. S., White S. D. M., 1996, *ApJ*, 462, 563
- Navarro J. F., Ludlow A., Springel V., Wang J., Vogelsberger M., White S. D. M., Jenkins A., Frenk C. S., Helmi A., 2010, *MNRAS*, 402, 21
- Okamoto T., Gao L., Theuns T., 2008, *MNRAS*, 390, 920
- Parkinson H., Cole S., Helly J., 2008, *MNRAS*, 383, 557
- Power C., Navarro J. F., Jenkins A., Frenk C. S., White S. D. M., Springel V., Stadel J., Quinn T., 2003, *MNRAS*, 338, 14
- Press W. H., Schechter P., 1974, *ApJ*, 187, 425
- Salvador-Sole E., Solanes J. M., Manrique A., 1998, *ApJ*, 499, 542
- Spergel D. N., Verde L., Peiris H. V., Komatsu E., Nolte M. R., Bennett C. L., Halpern M., et al. 2003, *ApJS*, 148, 175
- Springel V., Wang J., Vogelsberger M., Ludlow A., Jenkins A., Helmi A., Navarro J. F., Frenk C. S., White S. D. M., 2008, *MNRAS*, 391, 1685
- Springel V., White S. D. M., Frenk C. S., Navarro J. F., Jenkins A., Vogelsberger M., Wang J., Ludlow A., Helmi A., 2008, *Nature*, 456, 73
- Springel V., White S. D. M., Jenkins A., Frenk C. S., Yoshida N., Gao L., Navarro J., Thacker R., Croton D., Helly J., Peacock J. A., Cole S., Thomas P., Couchman H., Evrard A., Colberg J., Pearce F., 2005, *Nature*, 435, 629
- Tasitsiomi A., Kravtsov A. V., Gottlöber S., Klypin A. A., 2004, *ApJ*, 607, 125
- van Albada T. S., 1982, *MNRAS*, 201, 939
- Wechsler R. H., Bullock J. S., Primack J. R., Kravtsov A. V., Dekel A., 2002, *ApJ*, 568, 52
- White S. D. M., 1978, *MNRAS*, 184, 185
- Zhao D. H., Jing Y. P., Mo H. J., Börner G., 2003, *ApJ*, 597, L9